Technical Article

Homogenization and Model Order Reduction for Fast FE analysis

***Abstract* — When sing the standard FEM, it is still challenging to analyze the eddy currents in each strand of a Litz-wire and also each magnetic particle in soft magnetic composite. Because the radii of the strand and magnetic particle are much smaller than the device size, fine FE discretization necessary for the eddy current analysis results in quite a large equation system. This is a so-called multi-scale problem. In this article, it is shown that the homogenization method, which models material with fine structure as homogenous one with effective material constants, is fairly effective for the analysis of such multi-scale problems.**

Moreover, the standard FE analysis of electric apparatus such as motors and inductors need too long computational time to perform dynamic simulation coupled with power circuits. This article shows that the model order reduction can not only reduce the FE equations to accelerate the analysis but also allows us to synthesize the equivalent circuits directly from the FE equations which can easily be coupled with external circuits.

I. Introduction

The FE analysis of electric and electronic apparatus such as motors, transformers and inductors is now indispensable for their research and development. We can perform the design optimization and also three-dimensional field computations using FEM within acceptable duration of time. The standard FEM would need, however, unacceptably long computational time to analyze materials composed of multiple elements which are much smaller than the overall material size. For example, when we analyze the eddy currents in a Litz-wire which is composed of a number of stranded wires using the standard FEM, the resultant equation systems would be far too large to be solved in reasonable duration of time under usual computational environments. We encounter similar difficulty when computing the eddy current losses in the soft magnetic composite (SMC) which consists of many conductive magnetic particles coated by insulation layers. This article will show that the homogenization method is fairly effective for the eddy current analysis of these problems considering the skin and proximity effects. In this method, material such as multi-turn coil, Litz-wire and SMC is modeled as a homogenous material with macroscopic complex permeability. This method allows us, therefore, to perform the FE analysis with rather coarse FE meshes, and to reduce the computational time.

The standard FE analysis is also too time consuming to perform dynamic simulations of electric apparatus such as motors and inductors coupled with power circuits. For this reason, they are often analyzed with behavior modeling or equivalent circuits to reduce the computational time. These models can be realized by hardware to perform HILS (hardware-in-the-loop-simulation). However, it would be difficult to evaluate eddy current and hysteresis losses using these approaches. Moreover, the computational accuracy is sometimes unsatisfactory. In this article, it will be shown that the model order reduction (MOR) can be the alternative to these conventional methods. The MOR approach converts the original FE equation to reduced one with small number of unknowns. Moreover, MOR enables to synthesize the equivalent circuit of electric apparatus directly from its FE model.

In the next section, the homogenization method based on the macroscopic complex permeability will be formulated and the results of FE analysis of multi-turn coils and SMC will be reported. Moreover, the integral equation approach based on the complex permeability to perform three-dimensional analysis of Litz-wire will be described. In the third section, the MOR techniques will be surveyed and numerical results will be reported. Moreover, the synthesis of equivalent circuits based on MOR will be discussed. The last section provides the conclusions and outlooks.

II. Homogenization Methods

A. Analysis of multi-turn and Litz-wire coils [1]

When analyzing electric apparatus which has rich higher harmonics in the coil windings, the eddy current effects not only in the magnetic cores but also in wires have to be considered. There are two effects relevant to eddy currents: skin and proximity effects. The skin effect means that the eddy currents parallel to the wire axis are induced by the self-current so that the current concentrates near the wire surface. On the other hand, the proximity effect means that the anti-parallel eddy currents are induced by the magnetic fluxes generated by the ambient currents, and consequently the total current distribution becomes non-symmetric in the wire cross section. To reduce these effects, the Litz-wire composed of fine twisted strands is widely used. Figure 1 depicts the Litz-wire coil used for a wireless power transfer device.

In the conventional FE analysis of eddy currents in the multi-turn coils and in Litz-wire coils, the wires have to be subdivided into so fine elements that they are smaller than the skin depth. This results in large number of unknowns in the FE equation. Especially in the three-dimensional analysis, it would be difficult to solve the resultant large equation system even using high-performance computers. To circumvent this problem, the homogenization method which will be described below is fairly effective.

Fig. 1 Litz-wire coil
To reduce the eddy current losses, the Litz-wire coil is formed from many stranded fine wires.

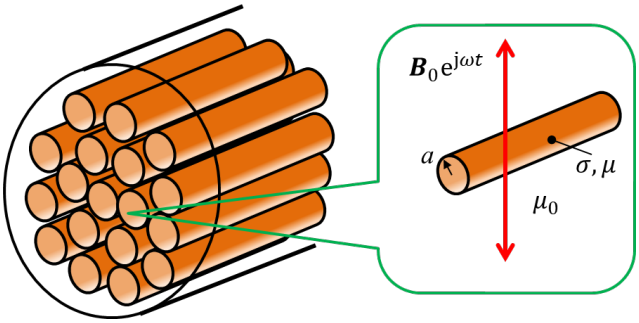

Fig. 2 Stranded wire and isolated wire in time-harmonic uniform field
A wire included in a bundle of stranded wires carrying alternating currents is modeled as an isolated wire immersed in a uniformed field generated by the surrounding wire currents.

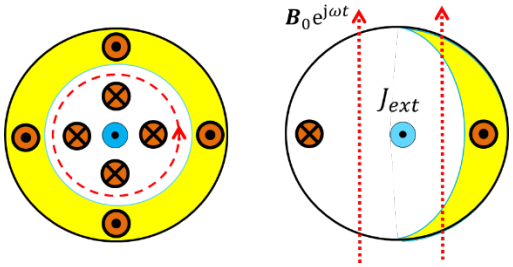

Fig. 3 Skin (left) and proximity (right) effects
Left: the circular magnetic flux (red) generated by the self-current (blue) induces the eddy currents (orange). As a result, the total current (yellow) concentrates near the wire surface. Right: The magnetic flux generated by surrounding currents induce the anti-parallel eddy currents. As a result, the total current (yellow) has the crescent-shaped distribution.

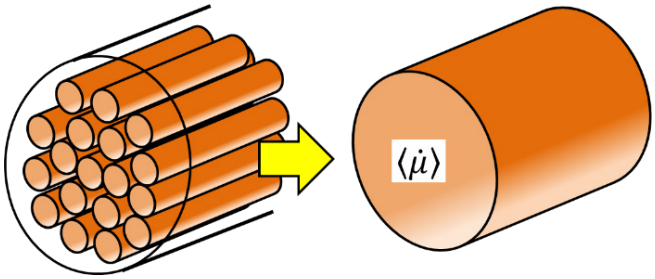

Fig. 4 Homogenization of stranded wires
The stranded wire is modeled as a homogenous material with the complex macroscopic permeability given by (8) defined on the wire cross section. For the three-dimensional analysis, the permeability tensor $[\mu] = \mathrm{diag}[\langle\dot{\mu}\rangle, \langle\dot{\mu}\rangle, \mu]$ is introduced, where μ is the original wire permeability.

Let us consider a bundle of wires composed of many parallel round conductors, as shown in Fig. 2, which carry alternating currents of angular frequency ω. The effect of twisting will be considered later. Let us pay attention to one of the conductors shown in the right. The magnetic field $\boldsymbol{B}_0$ in which this conductor is immersed would approximately be uniform, at least locally. This assumption is justified from the well-known fact that the magnetic field in a cylindrical hole in a cylindrical conductor carrying a uniform current is uniform [2].

The quasi-static fields inside and outside the wire can be analytically determined by solving the Maxwell equation. The fields inside the conductor can be written as

$$E_z = p_0 J_0(\zeta) + p_1 J_1(\zeta)\cos\theta\,, \qquad r \le a \qquad (1a)$$

$$H_\theta = \frac{jk}{\omega\mu}[p_0 J_1(\zeta) - p_1 J_1'(\zeta)\cos\theta], \qquad r \le a \qquad (1b)$$

where (r, θ, z) is the cylindrical coordinate in which z-axis is located along the wire axis, J_0 and J_1 denote the zeroth and first order Bessel functions, prime denotes derivative and $k = \sqrt{-j\omega\mu\sigma}, \zeta = kr$. The first and second terms in (1) express the fields relevant to the skin and proximity effects. The proximity effect means that the alternating fields generated by the surrounding wires induce the anti-parallel eddy currents in the wire as shown in Fig. 3. These eddy currents, which can be represented by a magnetic dipole moment $\boldsymbol{m}$, generate magnetic fields. Hence the eddy currents and magnetic dipole moment have to be determined self-consistently. Moreover, because the induced eddy currents are anti-parallel to each other, the distribution of the total current becomes non-symmetric as shown in Fig. 3 unlike the result of the skin effect. This non-symmetry is represented by the second terms in (1).

The fields outside the wire can be expressed as

$$E_z = \left(\frac{q_1}{r} + j\omega r B_0\right)\cos\theta\,, \qquad r \ge a \qquad (2a)$$

$$H_\theta = -\frac{j}{\omega\mu_0}\left(-\frac{q_1}{r^2} + j\omega B_0\right)\cos\theta\,, \qquad r \ge a \qquad (2b)$$

The first and second terms in (2) express the dipole field due to the proximity effect and the uniform external field, respectively. Note here that the components independent of θ, which will not be involved in the following discussions, are omitted for simplicity. The coefficient p_0 can be determined from the Ampere law for a given total current I : $p_0 = kI/(2\pi a\sigma J_1(\alpha)), \alpha = ka$, while p_1, q_1 can be determined from continuity in the tangential component of $\boldsymbol{E}$ and $\boldsymbol{H}$, that is

$$\begin{bmatrix} J_1(\alpha) & -1/a \\ \alpha J_1'(\alpha)/\mu_r & 1/a \end{bmatrix}\begin{bmatrix} p_1 \\ q_1 \end{bmatrix} = j\omega a B_0 \begin{bmatrix} 1 \\ 1 \end{bmatrix} \qquad (3)$$

The dipole fields, which represent the diamagnetic property due to the anti-parallel eddy currents along the wire, can also be expressed in terms of the magnetic dipole $\boldsymbol{m}$ in the form

$$A_z = -\frac{\mu_0}{2\pi}\frac{m}{r}\cos\theta \qquad (4)$$

By comparing the first term of (2a) and (4) where $E_z = -j\omega A_z$, we have the magnetization

$$M = \frac{m}{\pi a^2} = 2\pi\frac{B_0}{\mu_0}a^2\frac{\mu_r J_1(\alpha) - \alpha J_1'(\alpha)}{\mu_r J_1(\alpha) + \alpha J_1'(\alpha)} \qquad (5a)$$

By taking the static limit in (5), we obtain the well-known result for the magnetostatic field as

$$M = 2\frac{B_0}{\mu_0}\frac{\mu_r - 1}{\mu_r + 1} \qquad (5b)$$

Here let us define the complex permeability $\dot{\mu}$ so that (5b) holds at any frequency. To do so, we replace μ_r with $\dot{\mu}_r$ in (5b) and compare (5a) with (5b) to obtain

$$\dot{\mu}_r(\omega) = \mu_r\frac{J_1(\alpha)}{\alpha J_1'(\alpha)} = \frac{\mu_r}{\alpha\dfrac{J_0(\alpha)}{J_1(\alpha)} - 1} \qquad (6)$$

Now the proximity effect in a wire can be computed using (6) without fine FE discretization. However, FE discretization of the stranded wires and air region among them would still give rise to long computational time. To circumvent this problem, we use the homogenization method which models material composed of multiple elements as homogenous one.

It is known that the magnetostatic property of SMC can be evaluated at good accuracy [3] using the homogenized permeability given by

$$\langle \mu_r \rangle = 1 + \frac{\eta(\mu_r - 1)}{1 + N(1-\eta)(\mu_r - 1)} \tag{7}$$

where η and N denote the volume fraction (or filling rate) and diamagnetic constant which equals 1/2 for the round wire. Equation (7) is referred to as the Ollendorff formula [4] whose derivation is given in [1]. The Clausius-Mossotti formula based on the molecule field, often used for computation of homogenized permittivity of composite dielectric materials, and also the Maxwell-Garnett formula, used in microwave engineering, are shown equivalent to (7). The discussions on these equivalence are included in Ref. [1]. What we have to do to obtain the macroscopic complex permeability $\langle \dot{\mu} \rangle$ is just to substitute $\dot{\mu}_r$ in (6) into μ_r in (7). The result is

$$\langle \dot{\mu}_r(\omega) \rangle = 1 + \frac{2\eta(\dot{\mu}_r(\omega) - 1)}{2 + (1-\eta)(\dot{\mu}_r(\omega) - 1)} \tag{8}$$

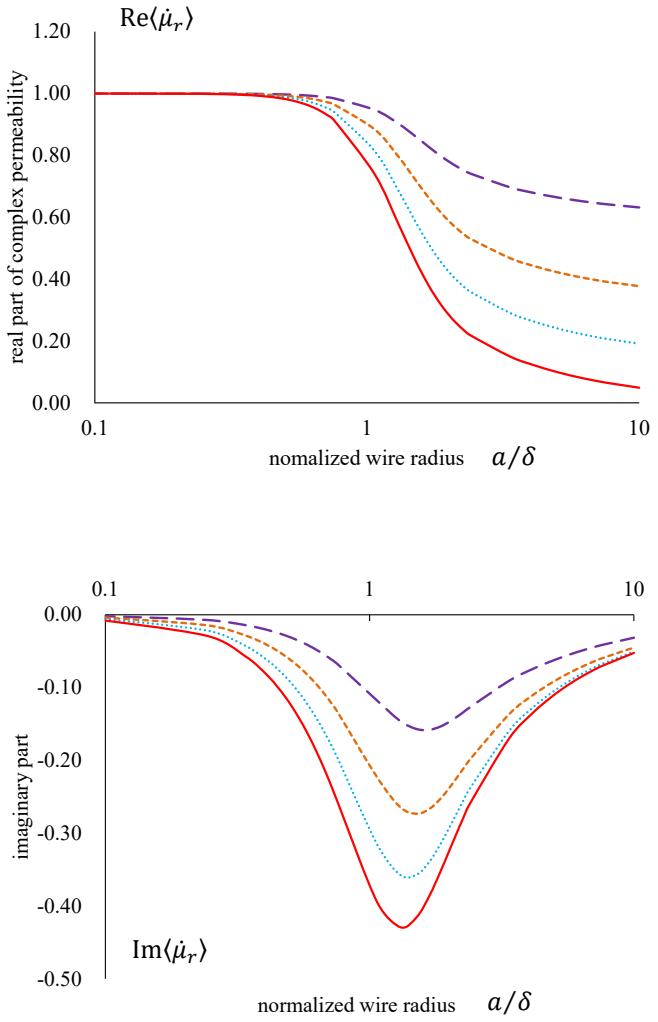

Fig. 5 Profiles of $\langle \dot{\mu}_r \rangle$ with different filling rates
The abscissa is the ratio of the wire radius a to the skin depth δ. The original wire permeability μ_r is set to 1. The red, blue, orange, purple curves are plotted for $\eta = 1, 0.75, 0.5, 0.25$.

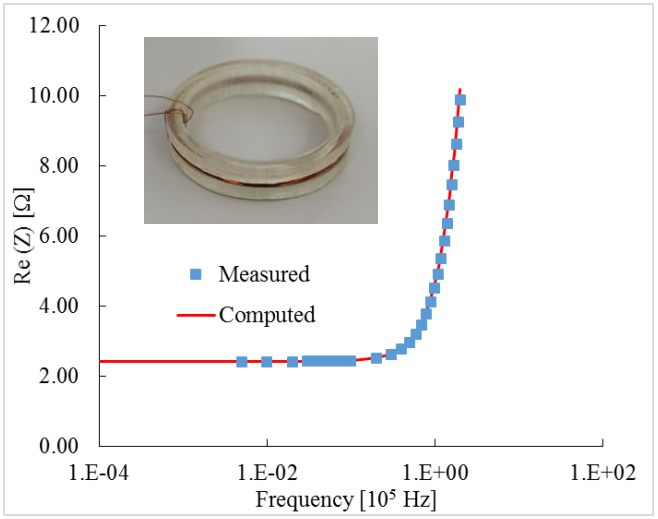

Fig. 6 Frequency dependence of 50-turned coil impedance
An enameled copper wire, radius 0.15 mm, cover thickness 0.03 mm is wound around a bobbin, radius 30 mm, manufactured by a 3D printer.

Now the stranded wire composed of fine wires can be modeled as a homogenous material as shown in Fig. 4. Note there that $\langle \dot{\mu}(\omega) \rangle$ is defined on the wire cross-section, whereas the permeability in the wire-axis direction can be approximated by the original permeability μ because the external magnetic flux along the wire axis would have little effects.

The frequency characteristics for different volume fractions are plotted in Fig.5, where the abscissa denotes the wire radius normalized by the skin depth $\delta = \sqrt{2/\mu\omega\sigma}$. The real and imaginary parts represent the permeability possessing the diamagnetic property due to the induced eddy currents and the eddy current loss, respectively. The former monotonously decreases with frequency, while the latter has a peak. This property is also found in the Debye relaxation of dielectric material. The reader would wonder that the curves for rather high values of η, which cannot be realized when using the round wires, are included in Fig. 5. Such a high filling rate can be realized when using the wire with square-shaped cross section whose diamagnetic constant N is also approximately 1/2.

For the test of this homogenization method, the impedance of 50-turned coil, shown in Fig. 6, has been experimentally measured and analyzed using the proposed method varying frequency for comparison. In the analysis, we solve the magnetostatic equation for the vector potential given by

$$\nabla \cdot (\nu \nabla A_z) = -J_z \tag{9}$$

on the plane containing the cross section of the coil. We use FEM where the permeability in the coil region is set to $\nu = 1/\langle \dot{\mu}(\omega) \rangle$ whereas $\nu = 1/\mu_0$ in the other regions. From the computed complex power,

$$\dot{P} = \frac{j\omega}{2} \int_{\Omega} \mu |\boldsymbol{H}|^2 \, dv + \frac{R_0 \, \alpha J_0(\alpha)}{4 J_1(\alpha)} |I|^2 \tag{10}$$

we compute the impedance $\dot{Z} = 2\mathrm{Re}(\dot{P})/I^2$, where R_0 is the dc-resistance of the wire. The real parts of the first and second terms in (10) represent the eddy current losses due to the proximity and skin effects, respectively. Note here that the eddy current losses and also its diamagnetic effects can be evaluated from magnetostatic analysis where the permeability in the coil region is simply replaced with (8). Of course, if there are other

conductors in which eddy currents flow, we have to solve the quasi-static electromagnetic equation instead of (9). However, also in this case, the coil region still can be modeled by (9). From the results plotted in Fig. 6, we conclude that the proposed method is sufficiently accurate.

Until now, we have considered parallel conductors. If the twisting pitch of stranded wires is sufficiently longer than the wire radius a, the above-mentioned method is valid. Unless this is the case, we have to consider the twisting effect. One of the possible ways to do so is to introduce the tensorial macroscopic complex permeability whose entities are determined from the wire direction. Namely, assuming that the stranded wires are locally parallel to each other, the permeability tensor is written as $[\mu] = \mathrm{diag}[\langle\dot{\mu}(\omega)\rangle, \langle\dot{\mu}(\omega)\rangle, \mu]$ in the local coordinates where the third axis is parallel to the wire. In the FE equation, this locally defined tensor is rewritten in the global coordinates. There is another way to treat the twisted wires; a conducting curved wire is modeled as a curved line on which one-dimensional integral equation is formulated. The latter method will be mentioned below.

B. One-dimensional Integral Equation [5]

As we have seen above, the proximity effect in a wire is modeled by the complex permeability (6), by which the FE discretization of the wire cross section is no more necessary. This means that the each wire can be modeled as a curved line on the plane perpendicular to which $\dot{\mu}$ and magnetization $\boldsymbol{M}$ generated by the anti-parallel eddy currents due to the proximity effect are defined (see Fig. 7). The proximity effect can be analyzed by determining $\boldsymbol{M}$ distributed along the curved line self-consistently. If we formulate the integral equation for $\boldsymbol{M}$ along the curved line, we do not need to consider the air region among the twisted wires. We know the magnetostatic integral equation for $\boldsymbol{M}$ in the magnetic material which is described in Ref. [6]. By extending this integral equation, we obtain the one-dimensional integral equation given by

$$\frac{\boldsymbol{M}(\boldsymbol{x})}{\dot{\mu}_r(\omega) - 1} = \boldsymbol{\tau} \times \left[\left(\int_{\Omega_w} g\boldsymbol{M}(\boldsymbol{x}')\, dv' + \boldsymbol{H}(\boldsymbol{x}') \right) \times \boldsymbol{\tau} \right] \tag{11a}$$

$$g\boldsymbol{M}(\boldsymbol{x}) = -\frac{1}{4\pi}\left[\frac{\boldsymbol{M}(\boldsymbol{x})}{R^3} - 3\frac{(\boldsymbol{M}(\boldsymbol{x}) \cdot \boldsymbol{R})\boldsymbol{R}}{R^5} \right] \tag{11b}$$

which describes the proximity effect in the stranded wires, where $\boldsymbol{\tau}, \Omega_w, \boldsymbol{H}$ denote the unit vector parallel to the wire, wire domain and external magnetic field, respectively, and $\boldsymbol{R} = \boldsymbol{x} - \boldsymbol{x}'$. Because $\boldsymbol{M}$ exists on the plane perpendicular to $\boldsymbol{\tau}$, we take the vector triple product in (11a). To numerically solve (11), we discretize the curved line into line segments to each of which $\boldsymbol{M}$ is assigned. The discretization of (11) leads to a system of equations containing a full matrix. This equation is can be effectively solved by iterative methods such as Jacobi and Gauss-Seidel methods.

After solving (11), we can evaluate the complex power from

$$\dot{P} = \frac{j\omega}{2} \int_{\Omega_w} \boldsymbol{J}^* \cdot \boldsymbol{A}\, dv + \frac{R_0\, \alpha J_0(\alpha)}{4\, J_1(\alpha)} |I|^2 \tag{12}$$

where $I, \boldsymbol{J}$ denote the total current and corresponding current density, and $\boldsymbol{A}$ is computed from

$$\boldsymbol{A}(\boldsymbol{x}) = \frac{\mu_0}{4\pi} \int_{\Omega_w} \left(\frac{\boldsymbol{M}(\boldsymbol{x}') \times \boldsymbol{R}}{R^3} + \frac{\boldsymbol{J}(\boldsymbol{x}')}{R} \right) dv' \tag{13}$$

Figure 8 shows the eddy current distribution in a multiple strand, shown in Fig. 7 (b), computed from $\boldsymbol{M}$ obtained by solving (11). Moreover, it is shown that the eddy current losses due to the proximity effect computed by this method and homogenization-based FEM mentioned in II.*A* are in good agreement [5]. It is stressed here that the method based on the one-dimensional integral equation can analyze Litz-wire three-dimensional structure. Moreover, this method is also valid even when there exit magnetic and conducting materials (see [5] for details). If there exit a number of twisted wires, say, more than one hundred, the simple discretization of (11) would impose large computational burden with respect to time and memory. We would introduce the fast multipole expansion or H-matrix method to solve this system.

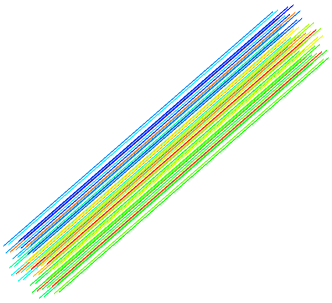

(a) parallel wires

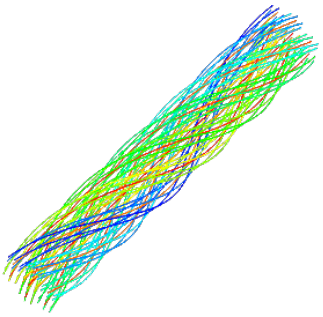

(b) multiple strand

Fig. 7 Modeling of stranded wires as curved lines. The magnetization M distributed along the curved lines can be determined by solving (11).

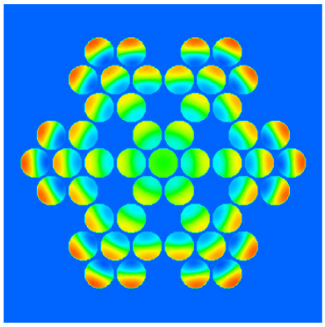

Fig. 8 Eddy current distribution in multiple strand composed of 49 wires After solving (11), the magnetic field $\boldsymbol{B}_0$ outside the wire is determined from $\boldsymbol{B}_0 = \mu_0\,(\dot{\mu}_r + 1)\boldsymbol{M}/2(\dot{\mu}_r - 1)$. Then, the unknown coefficient p_1 in (1a) can be determined from (3). The eddy currents in this figure are finally computed from $\boldsymbol{J} = \sigma\boldsymbol{E}$.

C. Time-domain Analysis [7]

We consider here how we apply the above-mentioned homogenization method to time-domain problems. This is required when we analyze, for example, the windings used in wireless power transfer devices which include nonlinear power circuits. Moreover, the present homogenization method can also be applied to SMC, as will be mentioned later. When we consider the magnetic nonlinearity in the magnetic particles in SMC, we also have to perform time-domain analysis.

The simplest way to do so would be to employ the convolution integral including the inverse Laplace transform of the reciprocal of $\langle\dot{\mu}\rangle$. The direct inverse Laplace transformation seems, however, uneasy. To circumvent this problem, let us consider the expansion of $\alpha J_0(\alpha)/J_1(\alpha)$ into contined fractions. The result is

$$\dot{\mu}_r(\omega) = \mu_r \cfrac{1}{2 - \cfrac{\alpha^2}{4 - \cfrac{\alpha^2}{6 - \cfrac{\alpha^2}{8 - \cdots}}}} \tag{14}$$

When we truncate the continued fraction in (14), we obtain the rational fraction which is referred to as the Padé approximation as follows:

$$\dot{\mu}_r = \mu_r \frac{c_0 + c_1 s + c_2 s^2 + \cdots + c_{q-1} s^{q-1}}{d_0 + d_1 s + d_2 s^2 + \cdots + d_q s^q} \tag{15}$$

where we replaced $j\omega$ with s. Substitution of (15) into the Offendorff formula (7) results in the partial fraction expansion of the form

$$\langle\dot{\nu}_r\rangle = \frac{1}{\langle\dot{\mu}_r\rangle} = \nu_\infty + \sum_{i=1}^{q} \frac{k_i}{s + p_i} \tag{16}$$

Now we can easily perform the inverse Laplace transform of (16) to obtain

$$\mathcal{L}^{-1}\langle\dot{\nu}_r\rangle = \nu_\infty \delta(t) + \sum_{i=1}^{q} k_i e^{-p_i t} \tag{17}$$

Applying (17) to the convolution integral, we can perform the time-domain analysis. In particular, we employ the RC method [8] by which the convolution integral can recursively be evaluated with reference to the field at just one previous time step. The authors have found that this approach gives numerical results which are in good agreement with those computed by the conventional FE analysis which requires very fine discretization.

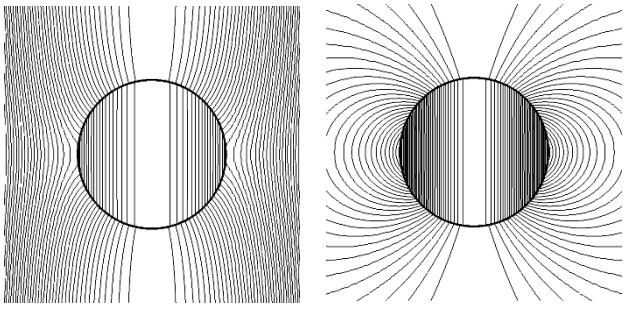

(c) real ($\delta/a = 5$) (d) imaginary ($\delta/a = 5$)

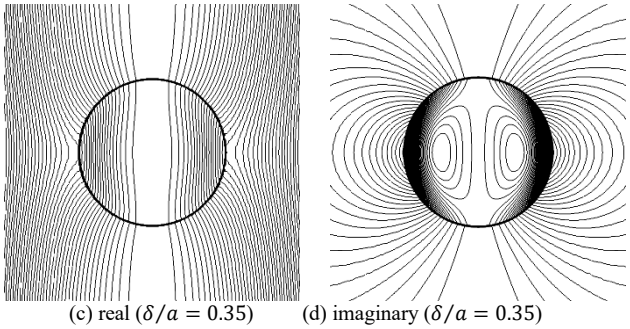

(c) real ($\delta/a = 0.35$) (d) imaginary ($\delta/a = 0.35$)

Fig. 9 Magnetic flux lines around a magnetic conductive particle immersed in uniform time-harmonic magnetic field, where a, δ denote the particle radius and skin depth [11].

D. Eddy Current Analysis of Soft Magnetic Composites [9, 10]

The soft magnetic composite, SMC, is composed of small iron particles embedded in insulation medium. Due to this structure, global eddy current cannot flow in SMC, and thus the eddy current loss can be suppressed. Moreover, SMC has another merit over the conventional silicon steel plates that three-dimensional shapes can easily be formed. For this reason, SMC has widely been used for inductors and reactors. However, as the driving frequency increases, the local eddy currents flowing in the iron particles come to give rise to non-negligible losses, which is also the case for the silicon steel sheets. Figure 9 shows the magnetic field distributions in an isolated iron particle for different frequencies.

The homogenization method mentioned above can also be applied to analysis of SMC considering the skin and proximity effects. Let us consider an isolated iron particle of radius a immersed in the uniform time-harmonic field $\boldsymbol{B}_0 e^{-j\omega t}$. Introducing the polar-coordinates (r, θ, ϕ) around the center of the particle, we can obtain the fields by analytically solving the quasi-static Maxwell equations as follows:

$$A_\phi = pB_0 i_1(\zeta)\sin\theta, \quad r \le a \tag{18a}$$

$$A_\phi = B_0\left(\frac{q}{r^2} + \frac{r}{2}\right)\sin\theta, \quad r \ge a \tag{18b}$$

where p, q are coefficients, $k = \sqrt{-j\omega\mu\sigma}, \zeta = kr$, and i_1 denotes the first-order modified Bessel function defined by

$$i_1(\zeta) = \frac{1}{\zeta^2}(\sin\zeta - \zeta\cos\zeta) \tag{19}$$

As in the same way for the stranded wires, the coefficients can be determined from the continuity condition in the electric and magnetic field on the particle surface, that is

$$\begin{bmatrix} i_1(\alpha) & -a^{-2} \\ -i_1(\alpha) + \sin(\alpha) & a^{-2} \end{bmatrix}\begin{bmatrix} p \\ q \end{bmatrix} = \frac{a}{2}\begin{bmatrix} 1 \\ 2 \end{bmatrix} \tag{20}$$

where $\alpha = ka$.

The magnetic field generated by a magnetic moment $\boldsymbol{m}$ in three-dimensional space can be written as

$$A_\phi = \frac{\mu_0}{4\pi}\frac{m}{r^2}\sin\theta \tag{21}$$

The first term in (18b) also expresses the dipole field, generated by the eddy currents in the particle. Hence, by comparing (18a) and (21), we find $m = 4\pi B_0 q/\mu_0$. The magnetization is then given by

$$M = \frac{3m}{4\pi a^3} = \frac{3B_0}{2\mu_0}\frac{(2\mu + \mu_0)i_1(\alpha) - \mu_0\sin\alpha}{(\mu - \mu_0)i_1(\alpha) + \mu_0\sin\alpha} \tag{22}$$

When taking the static limit $\omega \to 0$ in (22), we obtain the well-known result

$$M = \frac{3}{\mu_0}\frac{\mu - \mu_0}{\mu + 2\mu_0} \tag{23}$$

We again define the complex permeability $\dot{\mu}(\omega)$ so that (23) holds at any frequencies. From (22), (23), we finally obtain

$$\dot{\mu}_r(\omega) = \frac{2\mu_r(\alpha - \tan\alpha)}{(1-\alpha^2)\tan\alpha - \alpha} \tag{24}$$

This result has already been reported in Ref. [12]. By substituting (24) into the Ollendorff formula (7) where we set $N = 1/3$, we obtain the macroscopic complex permeability $\langle\dot{\mu}(\omega)\rangle$.

When we consider the magnetic saturation in the iron particles in SMC, we have to perform time-domain analysis. In this case, the inverse Laplace transform based on the Padé approximation given by (17) would be invalid because of the magnetic nonlinearity in μ. Instead, we compute the time-response of SMC using the Cauer-type ladder circuit, shown in Fig.10, which is directly synthesized from $\langle\dot{\mu}(\omega)\rangle$. In this synthesis, we expand (24) into a continued fraction using

$$\frac{\tan z}{z} = \cfrac{1}{1 - \cfrac{z^2}{3 - \cfrac{z^2}{5 - \cdots}}} \tag{25}$$

By substituting the resultant continued fraction into the Ollendorff formula, we have the rational polynomial of the form (15) for $\langle\dot{\mu}(\omega)\rangle$. Using the Euclidian algorithm, the rational polynomial can be expressed in the form of continued fraction

$$\langle\dot{\mu}\rangle = \cfrac{1}{L_1 - \cfrac{1}{\cfrac{R_1}{s} - \cfrac{1}{L_2 + \cdots}}} \tag{26}$$

This continued fraction corresponds to the Cauer circuit shown in Fig. 10. It is known [13, 14] that L_1 in the Cauer circuit is relevant to the primal magnetic field generated by an external current which usually overwhelms the fields generated by eddy currents. For this reason, by introducing proper nonlinear relationship between the flux and current in L_1, we can take the magnetic saturation in SCM particles into consideration. The circuit equation for the Cauer circuit in Fig.10, which is assigned in each finite element in the SMC region, is coupled with the FE equation. In Ref. [10], the time response of SMC computed by this approach has been shown to agree well with that computed by the unit-cell method. Figure 11 shows the magnetic distribution in the SMC core with and without considering the eddy currents in the iron particles. We can see the clear difference between these distributions.

E. Laminated Steel Sheets

We can also obtain the analytical expression of the macroscopic complex permeability $\langle\dot{\mu}\rangle$ for an infinitely wide iron sheet, shown in Fig.12, as follows:

$$\dot{\mu}_r(\omega) = \mu_r \frac{\tan\alpha}{\alpha} \tag{27}$$

where $\alpha = kd,\ k = \sqrt{-j\omega\mu\sigma}$, which is obtained by solving the one-dimensional quasi-static Maxwell equation

$$\frac{d^2H_z}{dx^2} + k^2H_z = 0 \tag{28}$$

Because the diamagnetic constant N nearly equals zero for the iron sheet, the Ollendorff formula (7) reduces to $\langle\dot{\mu}_r\rangle \approx \eta\dot{\mu}_r$. The Cauer circuit shown in Fig. 11 can also be synthesized from (27) [13]. It has been shown that the same Cauer circuit is

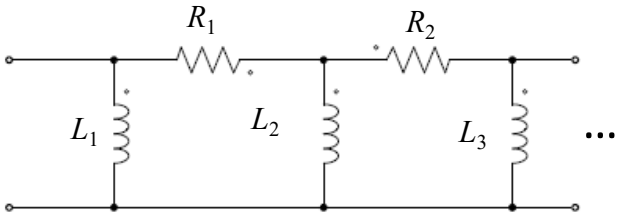

Fig. 10 Cauer circuit.

In the frequency domain, this circuit is equivalent to the macroscopic complex permeability of SMC given by (26). This circuit can be used for time domain analysis of SMC cores as well as laminated steel plates. Moreover, electric apparatus such as inductors and induction heating device can be modeled by the Cauer circuit as mentioned in III. *D*. In this case, the dc-resistance of the winding is inserted as R_0 in left of L_1.

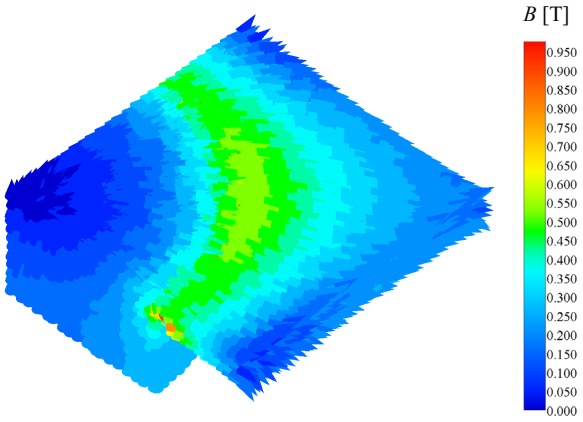

(a) with considering eddy current in SMC core

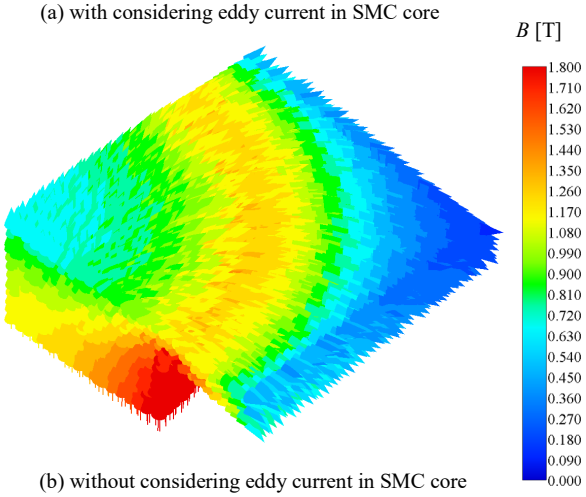

(b) without considering eddy current in SMC core

Fig.11 Magnetic fields in SMC core [see also 10].

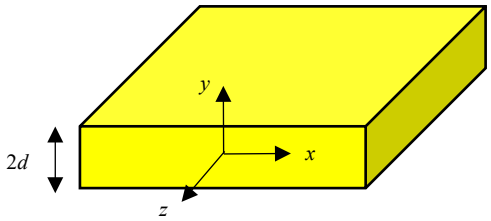

Fig. 12 A steel plate included in laminated steel sheets
The eddy current field can be determined by solving (23).

derived by expanding the magnetic field in (28) using the Legendre polynomials P_k as [15]

$$B_z(t,y) = \sum_{k=0,2,4\ldots} b_k(t) P_k(y/d) \qquad (29)$$

Moreover, the time-domain analysis [16] of the laminated steel sheets based on the expansion (29) has been shown equivalent to the circuit analysis using the Cauer circuit [15]. It is conjectured from this fact that in general the Cauer circuits synthesized from the complex permeability are always equivalent to those obtained from the field expansion using appropriate orthogonal polynomials. Furthermore, the synthesis of the Cauer circuits from quasi-static electromagnetic fields in arbitrary shaped domain is discussed in [17]. The Cauer circuit for the arbitrary quasi-static fields can also be synthesized using MOR, which will be described in III. *D*.

F. Unit-cell Approach

There is yet another homogenization method to analyze materials composed of multiple elements such as multi-turn coil and SMC, which is the unit-cell approach [18-21]. In this approach, material composed of multiple elements is assumed to consist of the same-sized unit cells, as shown in Fig. 13. The field in the unit cell is analyzed using, e.g., FEM under the boundary conditions considering the spatial periodicity. This method is advantageous over the method based on the complex permeability when the conductor included in the unit cell, such as a wire and particle, has arbitrary shapes. The drawback in the unit-cell method is that we have to perform FE analyses for different filling rates, frequencies and material constants unlike the method based on the complex permeability. In the frequency-domain analysis, the latter is, thus, advantageous when we consider simple shapes, such as circle and sphere, and also square and cuboid which can be approximated by the former two shapes. We can also obtain the macroscopic complex permeability $\langle \dot{\mu}(\omega) \rangle$ for arbitrary shaped materials based on the unit-cell approach with aid of MOR, which will be mentioned in III. *E*.

In the time-domain analysis using the unit-cell approach, we have to solve the one or two-dimensional quasi-static Maxwell equation in each finite element at all the time steps. This seems time consuming. If the system is linear, the RC method with Padé approximation is fairly effective because no field analysis is required. If the system is nonlinear, the Cauer-circuit approach, which is equivalent to the expansion with the Legendre polynomials, would be effective.

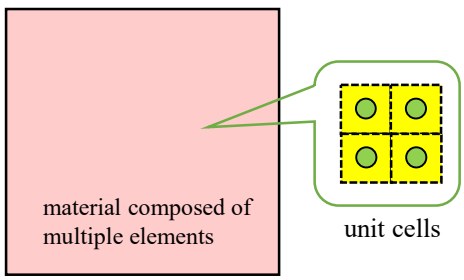

Fig. 13 Unit-cell approach.
It is assumed that the material composed of multiple elements consists of the same-sized unit cells. The field in each unit cell is numerically analyzed under adequate boundary conditions.

III. Model Order Reduction

A. Overview

In the design of electric apparatus, we often encounter the situations in which we have to the FE equation for many times changing material constants, shapes, configurations, frequencies and so on. In the design optimization based on FEM, the FE equation has to be solved for different parameters. When we solve the time-domain problems, we also repeatedly solve the FE equation at different time steps. MOR is quite useful to reduce the computational time in these situations.

One of the aims of MOR is to reduce the degree of freedoms (DoFs) in a given system [22]. For example, let us consider a humanoid which includes a lot of actuators. It would be uneasy to adequately control all the DoFs included in the humanoid in a coordinated manner. However, all the DoFs in various joints in a human body seem not to be linearly independent. This means that DoFs can be reduced without losing abilities to represent natural motion patterns. In the proper orthogonal decomposition (POD), which will be described in the following subsection, important DoFs are systematically extracted to reduce the system equation.

Another aim of MOR is to construct a simple expression for the input-output relation for a given system. When the relation is written in a rational polynomial in the *s*-domain, this corresponds to the Padé approximation. The rational polynomials can be obtained from POD and also via tri-diagonalization of the system matrix using, e.g., the Padé via Lanczos (PVL) method whose details will be described in III. *C*. The rational polynomials can also be obtained directly from the measured data or results of frequency sweep using, e.g., the vector fitting [23], and also by curve fitting based on optimization algorithms such as genetic algorithm (GA) and simulated annealing [24]. These MOR approaches, referred to as macro-modeling in microwave engineering [25], are schematically shown in Fig. 14.

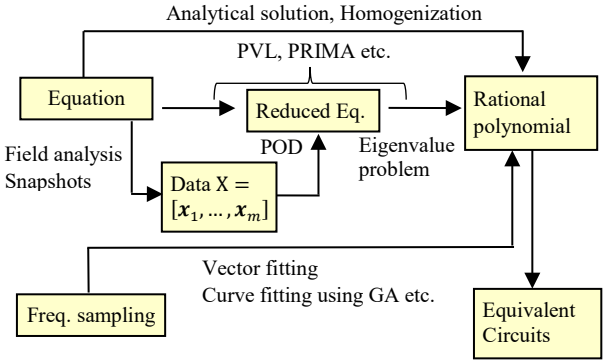

Fig. 14 Methods in model order reduction.

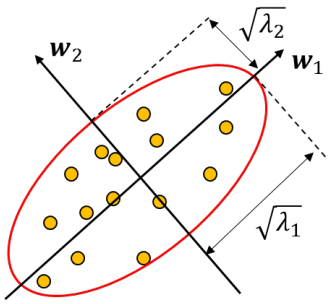

Fig. 15 Reduction of DoFs by POD.

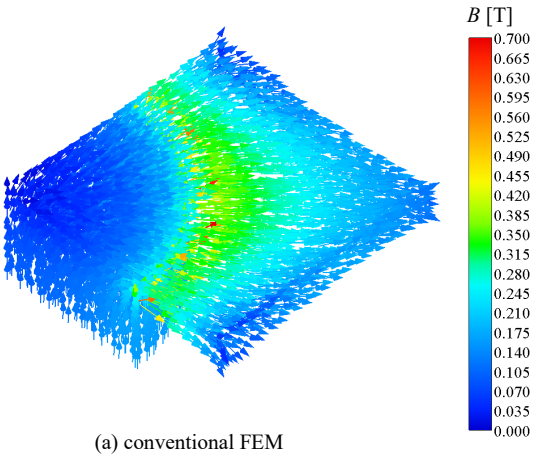

(a) conventional FEM

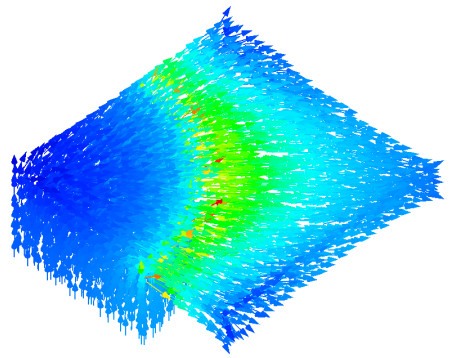

(b) POD

Fig. 16 Magnetic fields in iron core for weak current.

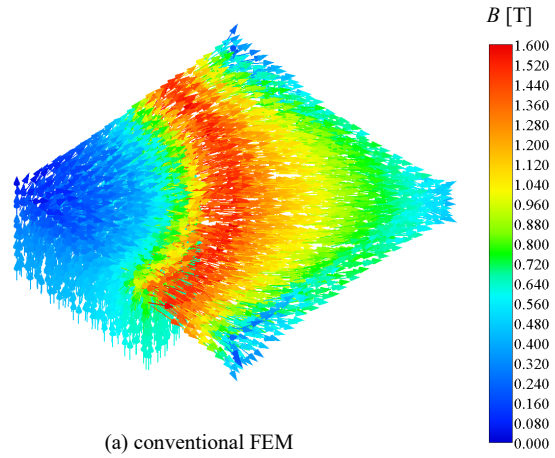

(a) conventional FEM

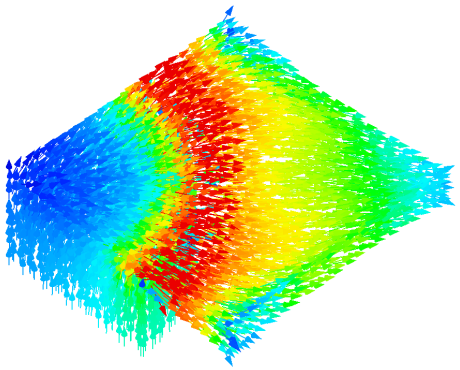

(b) POD

Fig. 17 Magnetic fields in iron core for strong current.

B. Proper Orthogonal Decomposition (POD)

Let us consider the linearly independent data $\boldsymbol{x}_i \in \mathbb{R}^n, i = 1,2 \dots, m$ which are represented by dots in Fig. 15. Assuming that they are obtained from $\boldsymbol{x}_i = \boldsymbol{x}_i' - \boldsymbol{\mu}$, where $\boldsymbol{x}_i', \boldsymbol{\mu}$ are the original data and their mean, the mean of $\boldsymbol{x}_i$ is set to zero. Moreover, we assume that $n \gg m$, which would hold, for example, when FE solutions with n DoFs are snapshotted at m points. If $\boldsymbol{x}_i$ distribute along an axis, they can be identified by referring their one-dimensional coordinate along the axis shown in Fig.15. The direction vector $\boldsymbol{w}$ of this coordinate axis can be found in such a way that the variation σ^2 of $\boldsymbol{x}_i$ projected on $\boldsymbol{w}$ becomes maximum. This can be mathematically expressed as

$$\sigma^2 = \boldsymbol{w}^{\mathrm{t}}\mathrm{S}\boldsymbol{w} \to \max., \qquad \text{sub. to } \|\boldsymbol{w}\|_2 = 1 \tag{30}$$

where S denotes the variance-covariance matrix defined by

$$\mathrm{S} = \frac{1}{m}\mathrm{X}\mathrm{X}^{\mathrm{t}}, \qquad \mathrm{X} = [\boldsymbol{x}_1, \boldsymbol{x}_2, \dots, \boldsymbol{x}_m] \in \mathbb{R}^{n\times m} \tag{31}$$

The matrix X is called the data matrix, which is included in Fig.14. The eigenvalue and corresponding eigenvectors of S are here denoted by $\lambda_1 \geq \lambda_2 \geq \cdots \geq \lambda_m, \boldsymbol{w}_1, \boldsymbol{w}_2, \dots, \boldsymbol{w}_m$. Note that because the rank of S is m, it has $n - m$ zero eigenvalues, which are omitted. The problem (30) is equivalent to

$$R = \frac{\boldsymbol{w}^t\mathrm{S}\boldsymbol{w}}{\boldsymbol{w}^t\boldsymbol{w}} \to \max. \tag{32}$$

It can be shown that $R \leq \lambda_1$, and, $R = \lambda_1$ when $\boldsymbol{w} = \boldsymbol{w}_1$. It is, therefore, concluded that $\boldsymbol{w}$ which satisfies (30) is just $\boldsymbol{w}_1$.

If $\boldsymbol{x}_i$ distribute within a three-dimensional ellipsoid, they can be identified by the coordinates along the elliptic axes. The direction vectors, orthogonal to each other, which span the three-dimensional space, are given by $\boldsymbol{w}_1, \boldsymbol{w}_2, \boldsymbol{w}_3$. Moreover, the elliptic radii along the axes are given by $\sqrt{\lambda_i}$. If $\lambda_1 \geq \lambda_2 \gg \lambda_3$, then it can be said that $\boldsymbol{x}_i$ almost distribute within a two-dimensional ellipsoid (ellipse). In this case, $\boldsymbol{x}_i$ can be expressed by the linear combination of the two major direction vectors. In general, if there are dominant k eigenvalues, we have the approximation

$$\boldsymbol{x} \approx \mathrm{W}\boldsymbol{y}, \qquad \mathrm{W} \in \mathbb{R}^{n\times k} \tag{33}$$

where $\mathrm{W} = [\boldsymbol{w}_1, \boldsymbol{w}_2, \dots, \boldsymbol{w}_k]$. The eigenvalues and eigenvectors can be obtained by the spectral decomposition of $\mathrm{X}^{\mathrm{t}}\mathrm{X}$ or performing the singular value decomposition of X. Since the vector $\boldsymbol{x}$ is expressed by the linear combination of the orthogonal bases, this method is called POD. The basis vectors are constructed from the snapshotted data in POD, while they are constructed by tri-diagonalization of the system matrix in PVL as will be shown in the next sub-section.

In POD applied to FE analysis, we perform frequency or time-domain analysis to obtain the snapshots $\boldsymbol{x}_i$ of the electromagnetic field [26, 27]. Then we compute W from X to reduce the FE equation, $\mathrm{K}\boldsymbol{x} = \boldsymbol{b}$, $\mathrm{K} \in \mathbb{C}^{n\times n}$, to

$$\mathrm{W}^{\mathrm{t}}\mathrm{K}\mathrm{W}\boldsymbol{y} = \mathrm{W}^{\mathrm{t}}\boldsymbol{b} \tag{34}$$

Now the number of unknowns is reduced from n to k. If $k \ll n$, the computational time for solution of the FE equation could drastically be reduced. Figures 16 and 17 show the magnetic field distributions computed by solving the original quasi-static FE equation and its reduced counterpart. They are in good agreement when the magnetic induction is weak. There exist,

however, small deteriorations between them when the magnetic induction is saturated.

When there are strong magnetic saturations in the magnetic core, it would be difficult to express the field as the linear combination of the form (33). Several remedies have been proposed for this problem. In Ref. [28, 29], POD is applied only to the linear domain which does not include saturating magnetic cores. In Ref. [30], the strongly saturated portions are extracted so that the field is interpolated by them in the discrete empirical interpolation method.

When analyzing electromagnetic fields around moving objects, we have to perform a lot of FE computations for different positions. Although the computational time could be reduced by employing POD, we would need many basis vectors to obtain accurate results because the fields have significant variations for different configurations. The block-MOR based on POD has been proposed to circumvent this difficulty [31]. In this method, all the possible configurations are classified into several gropes, and the different set of basis vectors is constructed for the configurations belonging to each grope. That is, the snapshots are subdivided into several blocks: $\mathrm{X} = [\mathrm{X}_1, \mathrm{X}_2, \dots]$. The basis matrix W_i is then constructed for X_i. The reduced FE equation $\mathrm{W}_i^{\mathrm{t}}\mathrm{K}\mathrm{W}_i\boldsymbol{y} = \mathrm{W}_i^{\mathrm{t}}\boldsymbol{b}$ is solved depending on the configuration. This method has extended to apply it to the analysis of rotating machines [32], which is shown in Fig. 18.

In the design optimization based on population-based methods such as GA and immune algorism, the field equation has to be solved for many times for fitness evaluations. To reduce the computational cost, POD has been applied to those optimizations [34]. In this method, the snapshots are taken by randomly changing the value of design parameters to construct the basis matrix W. The design optimization is carried out in which the reduced FE equation is solved. It has been shown that the computational time is reduced to about 10% when applying this method to antenna-shape optimization. Moreover, POD can also be used to synthesize the equivalent circuit from an FE model of electric apparatus. This will be mentioned in III. *D*.

C. Padé via Lanczos

In PVL [35], the Padé approximation of the transfer function is obtained on the basis of the Lanczos process which is widely used for eigenvalue computations. This method can avoid ill conditioning in the asymptotic waveform evaluation which directly determines the expansion coefficients of the transfer function. This section is devoted to formulation of PVL which is applied to the analysis of quasi-static electromagnetic fields.

Let us consider the quasi-static electromagnetic field coupled with electric circuits which are governed by

$$\kappa\frac{\partial \boldsymbol{A}}{\partial t} + \mathrm{rot}(\nu \mathrm{rot}\,\boldsymbol{A}) = I\boldsymbol{j} \tag{35a}$$

$$RI + L\frac{dI}{dt} + \frac{d\Phi}{dt} = V \tag{35b}$$

where $\boldsymbol{A}, \nu, \kappa, R, L, I, V$ are the vector potential, magnetic reluctivity, electric conductivity, resistance, inductance, current, voltage and $\Phi = \int \boldsymbol{A}\cdot\boldsymbol{j}dv$ is the magnetic flux. Moreover, $\boldsymbol{j}$ denotes the current direction vector defined by $\boldsymbol{j} = \boldsymbol{J}/I$, where $\boldsymbol{J}$ is the current density. Equation (35a) is discretized by FEM. The resultant FE equation as well as circuit equation (35b) can be written as a state and output equations as follows:

$$\mathrm{K}\boldsymbol{x} + \mathrm{N}\frac{d\boldsymbol{x}}{dt} = \boldsymbol{l}V \tag{36a}$$

$$I = \boldsymbol{l}^t\boldsymbol{x} \tag{36b}$$

where K, N denote the FE matrices, $\boldsymbol{x} \in \mathbb{R}^n$ is the unknown vector composed of the magneto-motive forces (integration of $\boldsymbol{A}$ along element edges) and I, and $\boldsymbol{l} = [0,0,..,0,1]^t$.

The Laplace transform of (36a) leads to the transfer function given by

$$H(s) = \boldsymbol{l}^t(\mathrm{K} + s\mathrm{N})^{-1}\boldsymbol{l} \tag{37}$$

which corresponds to the admittance function. We expand (37) around an expansion point s_0 to obtain

$$H(s_0 + \sigma) = \boldsymbol{l}^t(\mathrm{I} - \sigma\mathrm{A})^{-1}\boldsymbol{r} \tag{38}$$

where

$$\mathrm{A} = -(\mathrm{K} + s_0\mathrm{N})^{-1}\mathrm{N} \tag{39a}$$

$$\boldsymbol{r} = (\mathrm{K} + s_0\mathrm{N})^{-1}\boldsymbol{l} \tag{39b}$$

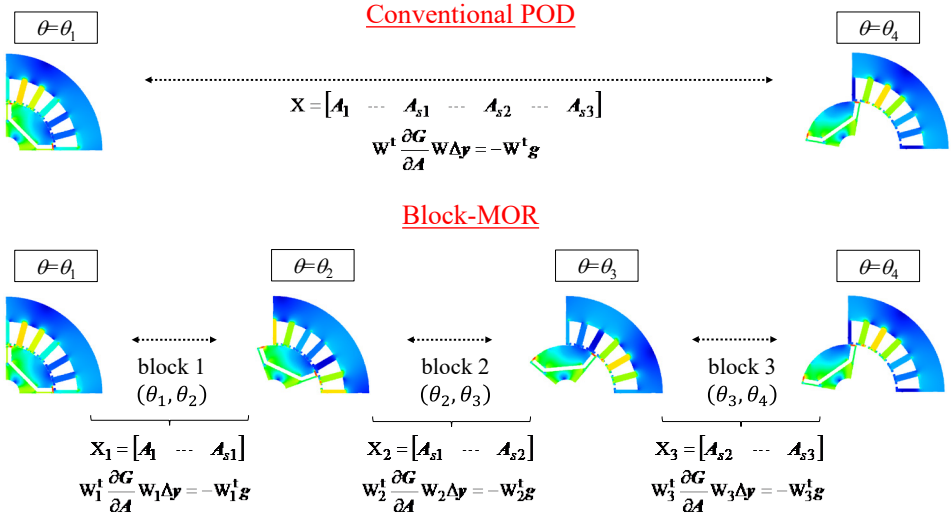

Fig.18 POD approaches for motor analysis [33].

It can be shown that A has real eigenvalues $\lambda_1 \geq \lambda_2 \geq \cdots \geq \lambda_n$ and diagonalizable with its orthonormal eigenvectors $\mathrm{U} = [\boldsymbol{u}_1, \boldsymbol{u}_2, \ldots, \boldsymbol{u}_n]$: $\mathrm{A} = \mathrm{U}\Lambda\mathrm{U}^{\mathrm{t}}$, where $\Lambda = \mathrm{diag}[\lambda_1, \ldots, \lambda_n]$. By diagonalization of A, (38) becomes

$$H(s_0 + \sigma) = \boldsymbol{f}^t(\mathrm{I} - \sigma\Lambda)^{-1}\boldsymbol{g} = \sum_{i=1}^{n} \frac{f_i g_i}{1 - \sigma\lambda_i} \tag{40}$$

where $f_i = \mathrm{U}^{\mathrm{t}}\boldsymbol{l}, g_i = \mathrm{U}^{\mathrm{t}}\boldsymbol{r}$. Now it is possible to easily compute the admittance from the rational function (40) at any frequency around s_0. It needs, however, large computational cost of order $O(n^3)$ to perform the diagonalization when the number of unknowns n is large as usual in FE analysis.

For this reason, we employ the Lanczos process which constructs the tri-diagonal matrix of order q, $q \ll n$, which approximates A. Since A is unsymmetric, we use the bi-Lanczos process, which generates the tri-diagonal matrices

$$\mathrm{T}_q = \begin{bmatrix} \alpha_1 & \beta_2 & 0 & & \\ \rho_2 & \alpha_2 & \beta_2 & & \\ 0 & \rho_3 & \alpha_3 & & \\ & & & \ddots & \\ & & & & \alpha_q \end{bmatrix} \tag{41a}$$

$$\tilde{\mathrm{T}}_q = \begin{bmatrix} \alpha_1 & \gamma_2 & 0 & & \\ \eta_2 & \alpha_2 & \gamma_2 & & \\ 0 & \eta_3 & \alpha_3 & & \\ & & & \ddots & \\ & & & & \alpha_q \end{bmatrix} \tag{41a}$$

and the basis vectors which satisfy

$$\mathrm{AV}_q = \mathrm{V}_q\mathrm{T}_q + [0,0,\ldots,\boldsymbol{v}_{q+1}]\rho_{q+1} \tag{42a}$$

$$\mathrm{A}^{\mathrm{t}}\mathrm{W}_q = \mathrm{W}_q\tilde{\mathrm{T}}_q + [0,0,\ldots,\boldsymbol{w}_{q+1}]\eta_{q+1} \tag{42b}$$

where $\mathrm{V_q} = [\boldsymbol{v}_1, \boldsymbol{v}_2, \ldots, \boldsymbol{v}_q]$, $\mathrm{W_q} = [\boldsymbol{w}_1, \boldsymbol{w}_2, \ldots, \boldsymbol{w}_q]$. The generated vectors are bi-orthogonal, that is, $\boldsymbol{v}_i \cdot \boldsymbol{w}_i = d_j$, $\boldsymbol{v}_i \cdot \boldsymbol{w}_j = 0, i \neq j$. From (42), it can be proved that $\mathrm{D}_q\mathrm{T}_q = \tilde{\mathrm{T}}_q^t\mathrm{D}_q$, $\mathrm{D}_q = \mathrm{diag}[d_1, d_2, \ldots, d_q]$.

The generated tri-diagonal matrix is an approximation of in the following sense: we consider the eigenvalue problem $\mathrm{A}\boldsymbol{x} = \lambda\boldsymbol{x}$. We assume that $\boldsymbol{x}$ can be approximated by the linear combination of $\boldsymbol{v}_i, i = 1,2,\ldots,q$, that is, $\boldsymbol{x} = \mathrm{V}_q\boldsymbol{y}$. Moreover, we apply the Galerkin method to the eigenvalue problem to obtain

$$\mathrm{W}_q^t(\mathrm{AV}_q\boldsymbol{y} - \lambda\mathrm{V}_q\boldsymbol{y}) = \mathrm{D}_q(\mathrm{T}_q\boldsymbol{y} - \lambda\boldsymbol{y}) = 0 \tag{43}$$

Hence by solving the small eigenvalue problem $\mathrm{T}_q\boldsymbol{y} = \lambda\boldsymbol{y}$, we obtain q approximated eigenvalues of A. Moreover, it can be shown that the transfer function (38) is expressed in terms of T_q as follows:

$$H(s_0 + \sigma) = \boldsymbol{l}^t\boldsymbol{r}\boldsymbol{e}_1^t(\mathrm{I} - \sigma\mathrm{T}_q)^{-1}\boldsymbol{e}_1 \tag{44}$$

Diagonalization of T_q in (44) leads to the partial fraction expansion, which is equivalent to the Padé approximation. This is the result of PVL.

D. Synthesis of equivalent circuits using MOR

It is shown in II. *D* that the Cauer circuit equivalent to the macroscopic complex permeability of SMC can be derived to realize time-domain analysis. The Cauer circuit equivalent to the FE model of electric apparatus can also be derived on the basis of MOR. Such an equivalent circuit can be analyzed much faster the FE equation. Moreover, it is possible to couple the equivalent circuits with the power and control circuits, and to analyze the overall performance using circuit simulators. In Ref. [36], the Cauer equivalent circuits for an air core coil and also an inductor are synthesized using PVL taking the eddy currents in the coil windings into account. Moreover, in Ref. [37], the Cauer equivalent circuit for an induction heating (IH) device is synthesized using POD.

Here let us consider the synthesis of the Cauer circuit from the FE model of an IH device [38], shown in Fig. 19, using PVL. In this IH device, the alternating current, 300 Hz, carried by the coil generates the magnetic flux which penetrates into the conducting plate. The eddy current induced by this magnetic flux generates Joule losses which increase the temperature of the conducting plate. By applying PVL to the FE equation (36a) which governs the IH device, we obtain the admittance function expressed in the rational polynomial of the form (44). As we do for $\langle\dot{\mu}(\omega)\rangle$ in II. *C*, we apply the Euclidean algorithm to rewrite the rational polynomial as a continued fraction. From this result, we can directly synthesize the Cauer circuit shown in Fig. 10, where R_0 is inserted in left of L_1, which is equivalent to the FE model of the IH device shown in Fig.19. Because the iron core has magnetic saturation, we introduce the nonlinear relationship between current and flux in L_1 of the Cauer circuit. In this circuit, R_0 represents the dc-resistance of the winding coil, while $R_k, L_k, k \geq 2$ represent the resistance and inductance relevant to the eddy current loss and fluxes generated by the eddy currents in the conducting plate. Figure 20 shows the time responses of the coil current in the IH device obtained from the synthetized Cauer circuit and corresponding FE equation. The amplitude of the alternating input voltage is set to 1V and 2V for Fig. 20 (a) and (b), respectively. When the amplitude is 1V, the current is almost sinusoidal, while it includes higher harmonics when the amplitude is increased to 2V due to the magnetic saturation in the iron core. In spite of existence in the waveform distortion in Fig. 20 (b), the Cauer circuit in which the magnetic nonlinearity is introduced in L_1, agrees well with that computed by FEM. Once the Cauer equivalent circuit is synthesized, simulation and design of the IH device coupled with the external control and power circuits can effectively be performed.

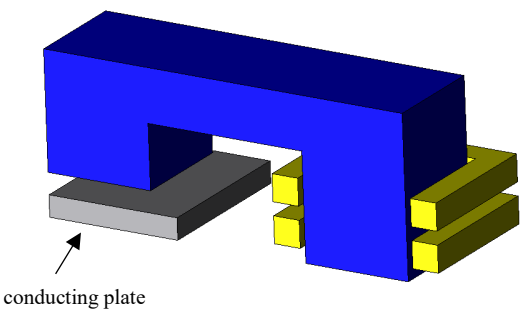

Fig. 19 Simple model of induction heating device.

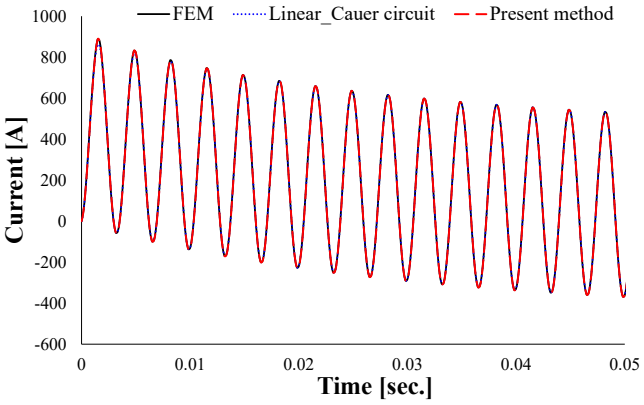

(a) input voltage: 1V

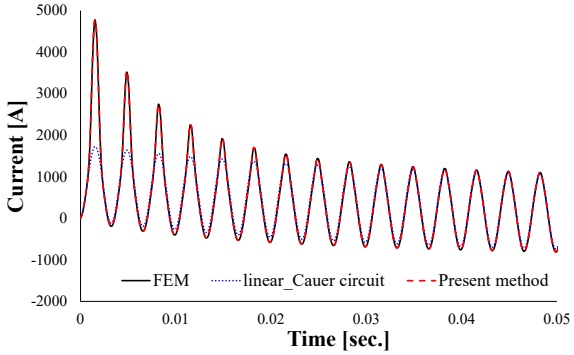

(b) input voltage: 2V

Fig. 20 Transient currents in windings in IH device
"linear_Cauer circuit" and "Present method" represent the results from the Cauer circuit, shown in Fig.11, without and with introducing the magnetic nonlinearity in L_1.

E. Homogenization using MOR

It is shown in II.*A* and II.*D* that the macroscopic complex permeability $\langle\dot{\mu}(\omega)\rangle$ of stranded wires and SMC can be obtained by substituting the complex permeability $\dot{\mu}(\omega)$, expressed in a closed form, into the Ollendorff formula (7). This method is valid when the inclusion shape is simple. It is, however, still possible to obtain $\langle\dot{\mu}(\omega)\rangle$ for arbitrary shaped inclusions such as ellipsoidal magnetic particles and wire with rectangular-shaped cross section using MOR. There are two possibilities to do so. In the first method, the magnetization M induced by eddy currents in an isolated inclusion immersed in time-harmonic magnetic field is analyzed using, e.g., FEM. The magnetization M, which can be formulated as a transfer function, is expressed as a rational function of s using either POD or PVL, which then is substituted into the Ollendorff formula (7) to obtain $\langle\dot{\mu}(\omega)\rangle$. In this computation, the demagnetization constant N of the inclusion has to be numerically determined. This method has been proposed and discussed in [39]. In the second method, the magnetization of the inclusion confined in a unit cell is analyzed using FEM and is then expressed as the rational function of s using either POD or PVL. In this case, $\langle\dot{\mu}(\omega)\rangle$ is obtained without introducing N although field computations have to be carried out to know its dependence on the filling factor η. This will be discussed elsewhere.

VI. Conclusions and Outlook

In this article, the homogenization method and MOR have been shown effective for reduction of computational cost in FE analysis of electromagnetic fields. The following problems remain for future studies.

(1) There is no experimental verification for the numerical method for modeling of Litz-wires mentioned in II.*B*. In particular, the dependence of eddy current loss and coil impedance on the twisting has to be studied by experiment and numerical computations.

(2) It is known that there exist electric and magnetic contacts among the magnetic particles used in SMC. It is necessary to take this effect into account for homogenization of SMC.

(3) It has been shown that the Cauer equivalent circuit can be constructed for laminated steel sheets, SMC cores well as stationary electric apparatus such as inductors and IH devices. It remains unclear if this method can be extended to modeling of rotating machines.

(4) The homogenization-based analysis of multi-turn coils and SMC cores can be performed based on the Padé approximation and Cauer equivalent circuit. The resulted algorithm is, however, rather complicated. Simplification of these methods would be required.

V. References

[1] H. Igarashi, "Semi-analytical approach for finite element analysis of multi-turn coil considering skin and proximity effects," *IEEE Trans. Magn*., vol.53, no.1, 7400107, 2017.

[2] L.D. Randau, L.P. Pitaevskii, E.M. Lifshitz, *Electrodynamics of Continuous Media*, Second Edition, Butterworth-Heinemann, 1979.

[3] Y. Ito, H. Igarashi, "Computation of macroscopic electromagnetic properties of soft magnetic composite", *IEEE Trans. Magn*., 49(5), pp. 1953-1956, 2013.

[4] F. Ollendorff, "Magnetostatik der Massekerne," *Arch. f. Eledtrotechnik*., 25, pp. 436-447, 1931.

[5] S. Hiruma, H. Igarashi, "Fast three-dimensional analysis of eddy current in Litz-wire using integral equation", presented at CEFC2016, to be published in *IEEE Trans. Magn.*

[6] P.P Silvester, R.L. Ferrari, *Finite elements for electrical engineers*, Cambridge University Press, 1996,

[7] Y. Sato, H. Igarashi, presented at Workshop "Advances in Multiscale Methods and Homogenization for Laminates and Windings in Magnetic Fields," 2016, to be submitted.

[8] R. Luebbers, *et al.*, "A frequency-dependent finite-difference time-domain formulation for dispersive materials," *IEEE Trans. Electromagnetic Compatibility,* vol.32, no. 3, pp.222-227, 1990.

[9] T. Sato, S. Aya, H. Igarashi, M. Suzuki, Y. Iwasaki, K. Kawano, "Loss computation of soft magnetic composite inductors based on interpolated scalar magnetic property," *IEEE Trans. Magn.*, vol. 51, Issue 3, March, 2015, Art. 8001704

[10] Y. Sato, H. Igarashi, "Time-domain analysis of soft magnetic composite using equivalent circuit obtained via homogenization", presented at CEFC2016, submitted to *IEEE Trans. Magn.*

[11] H. Igarashi, *et al.*, "Macroscopic magnetic property of soft magnetic composite considering eddy currents", (in Japanese) *IEEJ Technical Paper*, SA-14-075, RM-14-091, 2014

[12] A. Berthault, D. Rousselle, G. Zerah, “Magnetic properties of Permalloy microparticles,”*Journal of Magnetism and Magnetic Materials*, vol. 112, pp. 477-480, 1992.

[13] E. J. Tarasiewicz, A. S. Morched, A. Narang, E. P. Dick, “Frequency dependent eddy current models for nonlinear iron cores,” *IEEE Trans. on Power Systems*, vol.8 no.2 pp. 588-597, May, 1993.

[14] T. Miyazaki, T. Mifune, T. Matsuo, Y. Shindo, Y. Takahashi and K. Fujiwara, “Equivalent circuit modeling of dynamic hysteretic property of silicon steel under pulse width modulation excitation,” Journal of Applied Physics, 117, 17D110, 2015.

[15] Y. Shindo, T. Miyazaki, T. Matsuo, "Cauer circuit representation of the homogenized eddy-current field based on the legendre expansion for a magnetic sheet," *IEEE Trans. Magn.*, vol.52, no.3, Art. 6300504, 2015.

[16] J. Gyselinck, R.V. Sabariego, P. Dular, “A nonlinear time-domain homogenization technique for laminated iron cores in three-dimensional finite-element models,” *IEEE Trans. Magn*., vol. 42, pp. 763–766, 2006.

[17] Y. Shindo, A. Kameari, and T. Matsuo “High frequency nonlinear modeling of magnetic sheets using polynomial expansions for eddy-current field”, *IEEJ Trans. Power and Energy*, Vol.137, No.3, to be published, 2017

[18] A. Podoltsev and B. Lebedev, “Analysis of effective resistance and eddy current losses in multiturn winding of high-frequency magnetic components,” *IEEE Trans. Magn*., vol. 39, no. 1, pp. 539–548, 2003.

[19] J. Gyselinck and P. Dular, “Frequency-domain homogenization of bundles of wires in 2-D magnetodynamic FE calculations,” *IEEE Trans. Magn*., vol. 41, no. 5, pp. 1416–1419, 2005.

[20] H. Waki and H. Igarashi, “Estimation of effective permeability of magnetic composite materials”, *IEEE Trans. Magn*., 41, no. 5, pp. 1520-1523, 2005.

[21] Ito and H. Igarashi, “Computation of macroscopic electromagnetic properties of soft magnetic composite”, *IEEE Trans. Magn*., 49, no.5, pp. 1953-1956, 2013.

[22] W. H. Schilders, H. A. van der Vorst, J. Rommes (Eds.), *Model Order Reduction: Theory, Research Aspects and Applications*, Springer, 2008

[23] B. Gustavsen, A. Semlyen, "Rational approximation of frequency domain responses by vector fitting," *IEEE Trans. Power Delivery*, Vol. 14, No. 3, pp.1052-1061, 1999

[24] T. Shimotani, Y. Sato, H. Igarashi, "Equivalent-circuit generation from finite-element solution using proper orthogonal decomposition," *IEEE Trans. Magn.*, vol. 52, vol. 3, Art. 7206804, 2016.

[25] R. Achar, M.S. Nakhla, Simulation of high-speed interconnects, *Proceedings of the IEEE*, Vol.89, no.5, pp.693 - 728, 2002.

[26] D. Schmidthäusler, M. Clemens, "Low-order electroquasistatic field simulations based on proper orthogonal decomposition," *IEEE Trans. Magn*., vol.48, no.2, pp.567-570, 2012

[27] Y. Sato, H. Igarashi, "Model reduction of three-dimensional eddy current problems based on the method of snapshots," *IEEE Trans. Magn*., vol. 49, no.5, pp.1697-1700, 2013

[28] D. Schmidthausler, S. Schops, M. Clemens, "Linear subspace reduction for quasistatic field simulations to accelerate repeated computations," *IEEE Trans. Magn.* vol.50, no.2, Art. 7010304, 2014.

[29] Y. Sato, M. Clemens, H. Igarashi, "Adaptive subdomain model order reduction with discrete empirical interpolation method for nonlinear magneto-quasi-static problems," *IEEE Trans. Magn*., vol. 52, vol. 3, Art. 1100204, 2016.

[30] T. Henneron, S. Clénet, Model order reduction of non-linear magnetostatic problems based on POD and DEI methods, IEEE Trans. Magn. vol.50, no.2, Art. 7000604, 2014

[31] T. Sato, Y., Sato, H. Igarashi, "Model order reduction for moving objects: fast simulation of vibration energy harvesters," *COMPEL*, vol. 34, no.5, 2015.

[32] T. Shimotani, Y. Sato, T. Sato, Hajime Igarashi, "Fast finite-element analysis of motors using block model order reduction," *IEEE Trans. Magn*., vol. 52, vol. 3, Art. 7207004, 2016.

[33] T. Shimotani, Y. Sato, Hajime Igarashi, “Acceleration of Motor Analysis Using Block Model Order Reduction”, (in Japanese), *IEEJ Technical Report*, SA-15-099, RM-15-137, 2015.

[34] Y. Sato, F. Campelo, H. Igarashi, "Fast shape optimization of antennas using model order reduction," *IEEE Trans. Magn.* vol. 51, no. 3, 2015, Art. 7204304.

[35] P. Feldmann and R. A. Freund, "Efficient linear circuit analysis by Pade approximation via the Lanczos process," *IEEE Trans. Computer-Aided Design*, vol. 14, no. 5 pp. 639-649, 1995.

[36] Y. Sato, H. Igarashi, "Generation of equivalent circuit from finite element model using model order reduction," *IEEE Trans. Magn.*, vol. 52, no. 3, Art. 1100304, 2016.

[37] T. Shimotani, Y. Sato, H. Igarashi, “ Direct synthesis of equivalent circuits from reduced FE models using proper orthogonal decomposition, ” *COMPEL*, vol. 35, no. 6, pp. 2035-2044, 2016.

[38] Y. Sato, T. Shimotani, H. Igarashi, "Synthesis of Cauer-equivalent circuit based on model order reduction considering nonlinear magnetic property", presented at CEFC2016, submitted to *IEEE Trans. Magn*.

[39] Y. Sato, H. Igarashi, "Homogenization method based on model order reduction of FE analysis of multi-turn coils", presented at CEFC2016, submitted to *IEEE Trans. Magn*.

AUTHORS NAME AND AFFILIATION

Hajime Igarashi, Yuki Sato, Shogo Fujita, Shingo Hiruma, Yoshitsugu Otomo

Hokkaido University, Japan
Kita 14, Nishi 9, Kita-ku, Sapporo, 060-0814
igarashi@ssi.ist.hokudai.ac.jp